

**Electronic Supplementary Information for
Hierarchical NiCo₂O₄@NiMoO₄ Core-Shell Hybrid
Nanowire/nanosheet Arrays for High-Performance
Pseudocapacitors**

Ding Cheng^{a,b}, Yefeng Yang^{a,b,d*}, Jinlei Xie^{a,c}, Changjiang Fang^{a,b}, Guoqing Zhang^b, and Jie Xiong^{a,b*}

*a Department of Materials Engineering, College of Materials and Textile,
Zhejiang Sci-Tech University, Hangzhou 310018, P. R. China*

*b MOE Key Laboratory of Advanced Textile Materials and Manufacturing
Technology, Zhejiang Sci-Tech University, Hangzhou 310018, P. R. China*

*c Qixin Honors College, Zhejiang Sci-Tech University, Hangzhou 310018, P.
R. China*

*d State Key Lab of Silicon Materials, Zhejiang University, Hangzhou
310027, P. R. China*

Email address: yangyf@zstu.edu.cn (Dr. Y. Yang);

jxiong@zstu.edu.cn (Prof. J. Xiong)

Tel: +86-571-8684 3586

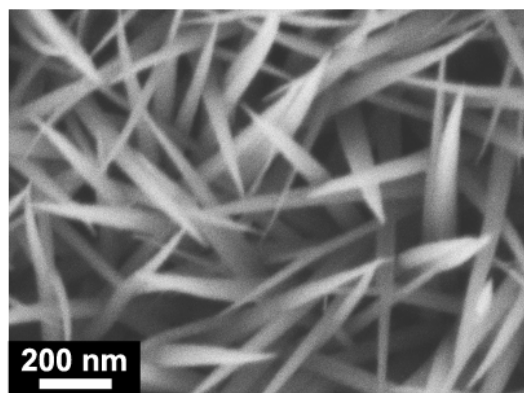


Figure S1. High magnification SEM image of pristine NiCo_2O_4 NWAs on the Ni foam substrate.

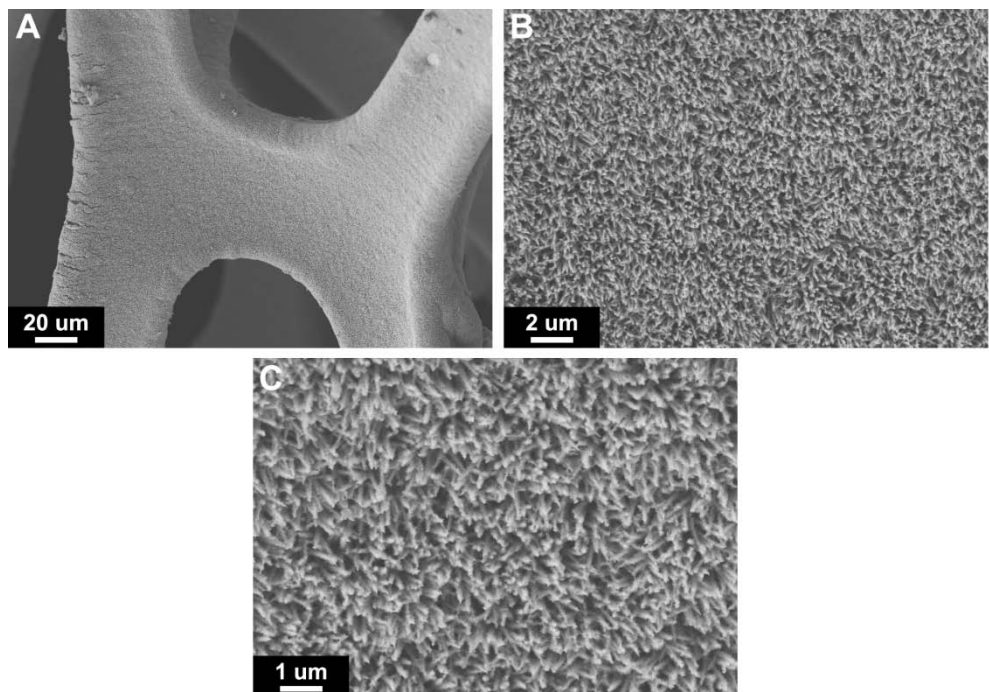


Figure S2. Additional SEM images of the $\text{NiCo}_2\text{O}_4@\text{NiMoO}_4$ core-shell hybrid NWSAs (4 h) in different magnifications, indicating the formation of the core-shell hybrid nanostructures in a large scale on Ni foam.

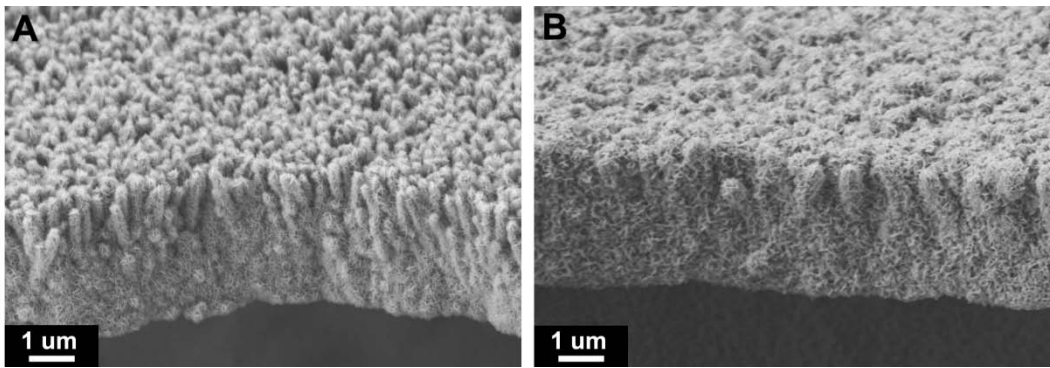


Figure S3. Typical cross-sectional SEM images of $\text{NiCo}_2\text{O}_4@\text{NiMoO}_4$ core-shell hybrid NWSAs on Ni foam substrate obtained at different reaction time: (A) 8 h, and (B) 12 h, respectively.

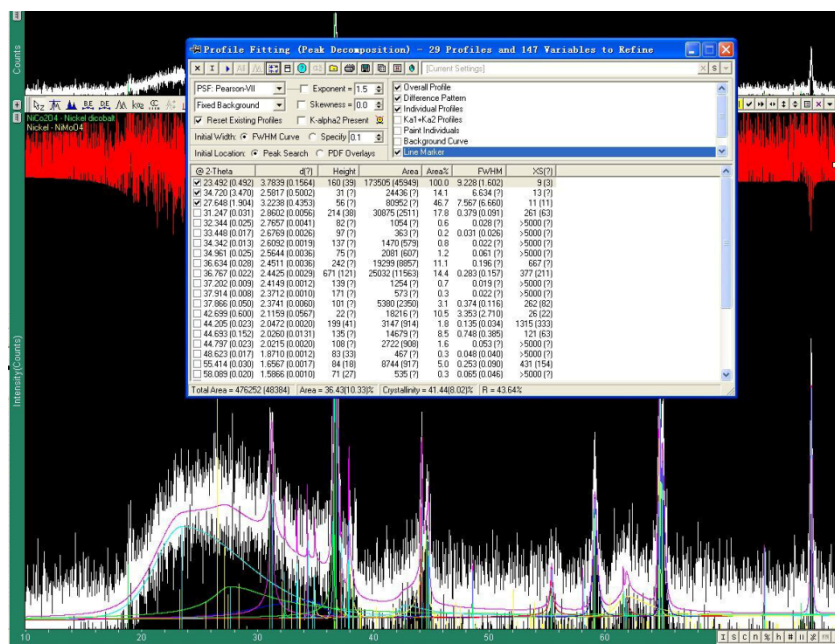


Figure S4. The fitting results of the XRD pattern recorded from $\text{NiCo}_2\text{O}_4@\text{NiMoO}_4$ hybrid NWSAs (16 h).

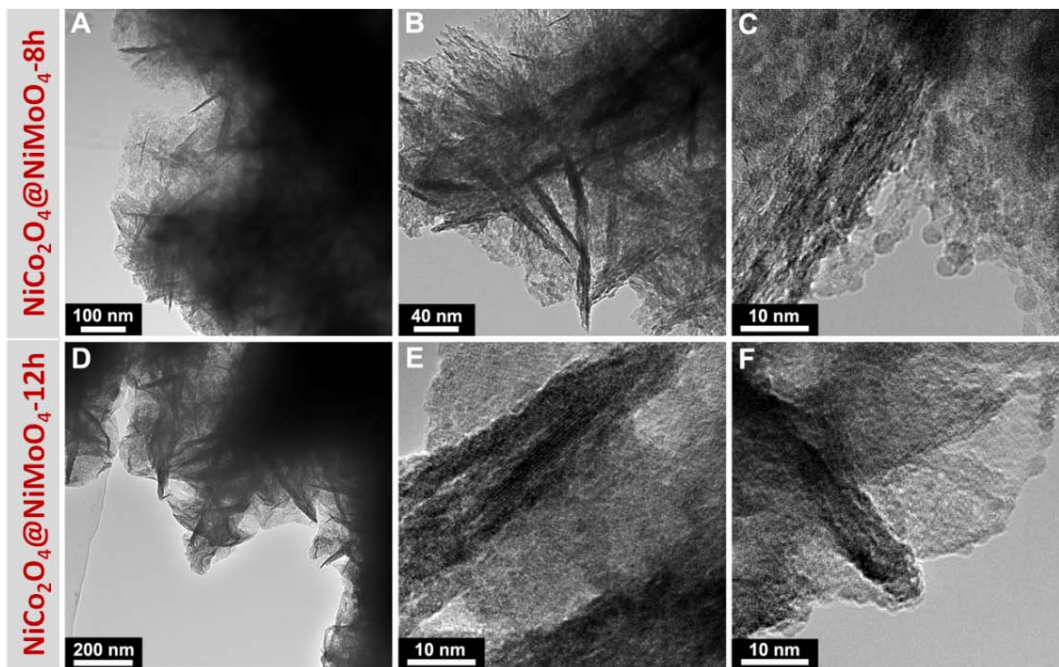


Figure S5. Typical TEM and HRTEM images of the shell regions from the $\text{NiCo}_2\text{O}_4@\text{NiMoO}_4$ core-shell hybrid NWSAs obtained at different reaction time: (A-C) 8 h and (D-F) 12 h, respectively.

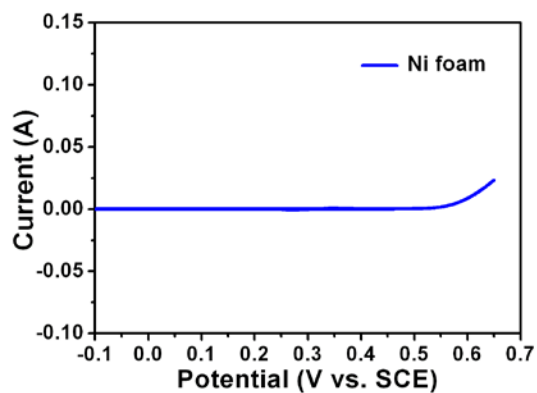


Figure S6. CV curve of bare Ni foam measured at a scan rate of 5 mV/s.

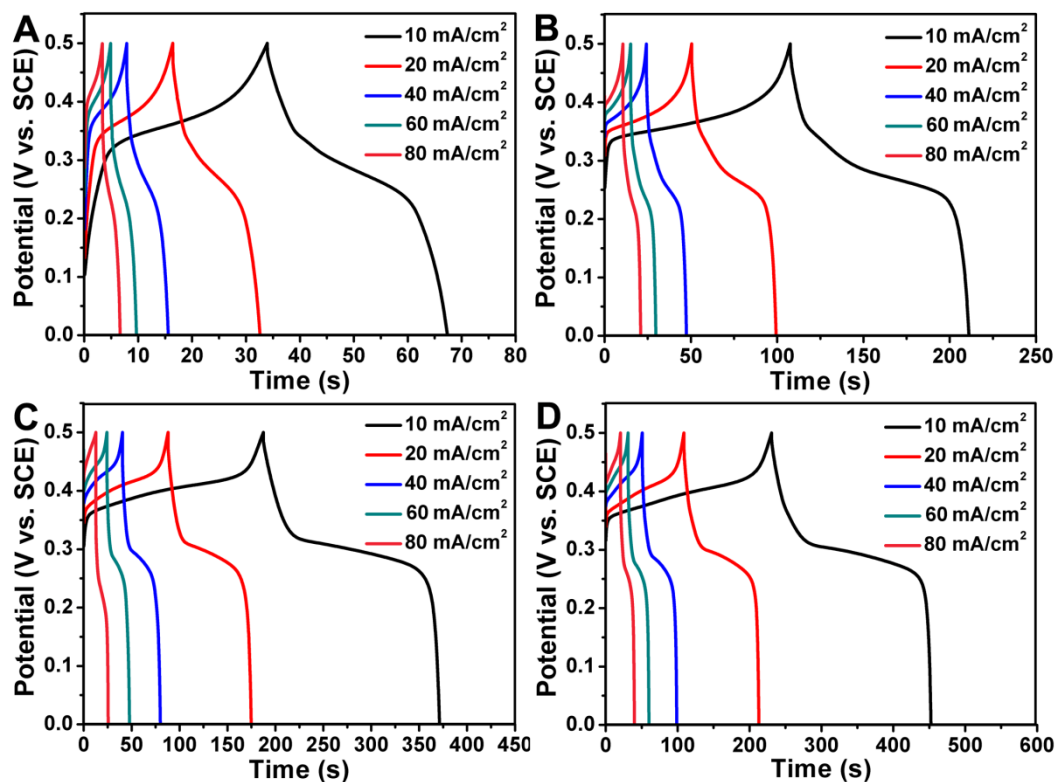


Figure S7. Galvanostatic charge-discharge curves of (A) pristine NiCo_2O_4 and (B-D) $\text{NiCo}_2\text{O}_4@\text{NiMoO}_4$ hybrid electrodes with different reaction time of NiMoO_4 : (B) 4 h, (C) 8 h, and (D) 16 h, respectively.

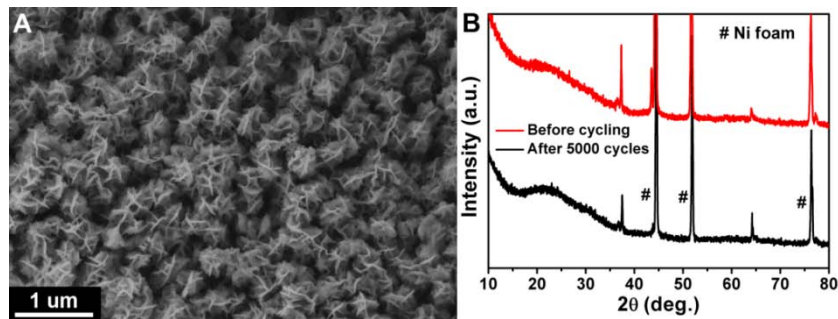


Figure S8. (A) Typical SEM image and (B) corresponding XRD pattern of the optimized $\text{NiCo}_2\text{O}_4@\text{NiMoO}_4$ hybrid electrode (12 h) on Ni foam after 5000 cycles. The XRD pattern of this hybrid electrode before cycling is also included for comparison. These results clearly confirm the morphological and structural stability of the hybrid sample during the long-term cycling process. Besides, the mass change of loaded hybrid materials is observed to be nearly negligible. It should be pointed out that due to the limited amount of electroactive materials on Ni foam (1 cm*1 cm) for cycling test, the XRD pattern of the hybrid sample after cycling is directly recorded on Ni foam substrate.

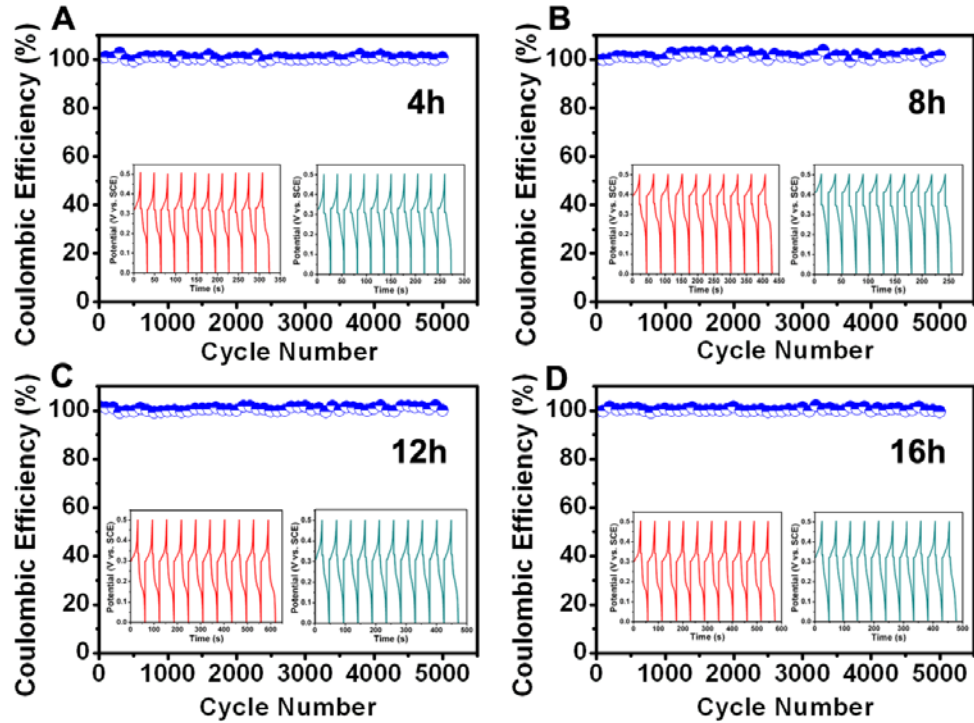


Figure S9. Coulombic efficiency variation of the $\text{NiCo}_2\text{O}_4@\text{NiMoO}_4$ hybrid NWSAs with different reaction time during the cycling at the current density of $50 \text{ mA}/\text{cm}^2$: (A) 4 h, (B) 8 h, (C) 12 h, and (D) 16 h, respectively. The inset shows the corresponding charge-discharge curves of the first and last 10 cycles for each electrode.

Table S1. Comparison of the electrochemical performance of the $\text{NiCo}_2\text{O}_4@\text{NiMoO}_4$ hybrid NWSAs and other 3D core-shell electrode materials reported in literatures.

Electrodes based on materials	Areal (specific) capacitance	Rate capability	Cycling stability	Ref.
$\text{NiCo}_2\text{O}_4@\text{MnO}_2$ nanowire arrays	3.31 F/cm ² at 2 mA/cm ²	50.2% retention at 20 mA/cm ²	88% retention after 2000 cycles at 10 mA/cm ²	1
$\text{NiCo}_2\text{O}_4@\text{MnO}_2$ nanowire arrays	2827 F/g at 2 mA/cm ²	76.4% retention at 50 mA/cm ²	98.4% retention after 3000 cycles at 10 mA/cm ²	2
$\text{NiCo}_2\text{O}_4@\text{Ni}_3\text{S}_2$ nanothorn arrays	1716 F/g at 1A/g	64.3% retention at 20 A/g	83.7% retention after 2000 cycles at 4 A/g	3
$\text{NiCo}_2\text{O}_4@\text{NiCo}_2\text{O}_4$ nanoflake arrays	1.55 F/cm ² at 2 mA/cm ²	74.8% retention at 40 mA/cm ²	98.6% retention after 4000 cycles at 5 mA/cm ²	4
$\text{NiCo}_2\text{O}_4@\text{NiCo}_2\text{O}_4$ nanosheet/nanorod arrays	1925 F/g at 0.5 A/g	76.4% at 20 A/g	90.1% retention after 3500 cycles at 5 A/g	5
$\text{NiCo}_2\text{O}_4@\text{Ni}_{x}\text{Co}_{1-x}(\text{OH})_2$ nanowire/nanosheet arrays	1.64 F/cm ² at 2 mA/cm ²	67% retention at 90 mA/cm ²	81.3% retention after 2000 cycles at 2 mA/cm ²	6
$\text{Co}_3\text{O}_4@\text{NiMoO}_4$ nanowire arrays	6.40 F/cm ² at 10 mA/cm ²	78.9% retention at 80 mA/cm ²	77% retention after 3000 cycles at 50 mA/cm ²	7
$\text{NiO}@ \text{CoMoO}_4$ nanocomposites	848 F/g at 0.5 A/g	75.1% retention at 8 A/g	100% retention after 3000 cycles 8 A/g	8
$\text{Co}_3\text{O}_4@\text{NiMoO}_4$ nanosheet arrays	2.67 F/cm ² at 3 mA/cm ²	72% retention at 30 mA/cm ²	70% retention after 1000 cycles at 15 mA/cm ²	9
$\text{MnMoO}_4@\text{CoMoO}_4$ nanocomposites	204.1 F/g at 0.5 A/g	66% retention at 3 A/g	98% retention after 1000 cycles at 20 A/g	10
$\text{NiMoO}_4@\text{MnO}_2$ nanowire/nanoflake arrays	3.90 F/cm ² at 8 mA/cm ²	82.5% retention at 24 mA/cm ²	90.5% retention after 4000 cycles at 24 mA/cm ²	11
$\text{NiCo}_2\text{O}_4@\text{CoMoO}_4$ nanowire/nanoplate arrays	14.67 F/cm ² at 10 mA/cm ²	65.8% retention at 60 mA/cm ²	74.1% retention after 1000 cycles at 60 mA/cm ²	12
$\text{NiCo}_2\text{O}_4@\text{NiMoO}_4$ nanowire/nanosheet arrays	5.80 F/cm ² at 10 mA/cm ²	83.6% retention at 80 mA/cm ²	81.8% retention after 5000 cycles at 50 mA/cm ²	This work

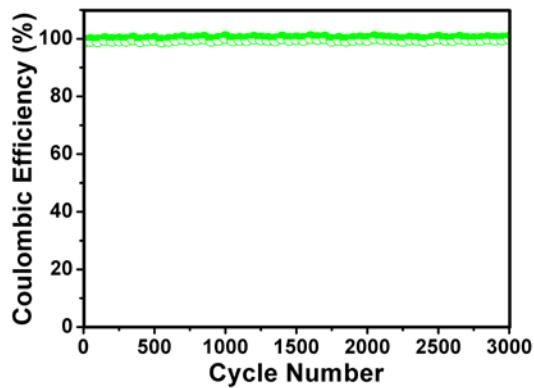


Figure S10. Coulombic efficiency of the $\text{NiCo}_2\text{O}_4@\text{NiMoO}_4$ (12 h)//AC asymmetric supercapacitor during the cycling at the current density of 20 mA/cm^2 .

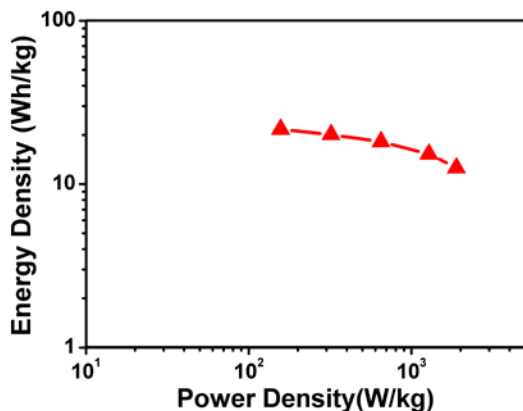


Figure S11. Ragone plot of the ASC device relating the gravimetric energy density and power density.



Figure S12. Digital photo of two ASCs connected in series that can power a commercial digital meter brightly after charging for 5 min.

References:

1. L. Yu, G. Q. Zhang, C. Z. Yuan and X. W. Lou, *Chemical Communications*, 2013, **49**, 137-139.
2. R. J. Zou, M. F. Yuen, Z. Y. Zhang, J. Q. Hu and W. J. Zhang, *Journal of Materials Chemistry A*, 2015, **3**, 1717-1723.
3. J. P. Wang, S. L. Wang, Z. C. Huang and Y. M. Yu, *Journal of Materials Chemistry A*, 2014, **2**, 17595-17601.
4. X. Y. Liu, S. J. Shi, Q. Q. Xiong, L. Li, Y. J. Zhang, H. Tang, C. D. Gu, X. L. Wang and J. P. Tu, *ACS Applied Materials & Interfaces*, 2013, **5**, 8790-8795.
5. W. W. Zhou, D. Z. Kong, X. T. Jia, C. Y. Ding, C. W. Cheng and G. W. Wen, *Journal of Materials Chemistry A*, 2014, **2**, 6310-6315.
6. L. Huang, D. C. Chen, Y. Ding, S. Feng, Z. L. Wang and M. L. Liu, *Nano Letters*, 2013, **13**, 3135-3139.
7. D. P. Cai, D. D. Wang, B. Liu, L. L. Wang, Y. Liu, H. Li, Y. R. Wang, Q. H. Li and T. H. Wang, *ACS Applied Materials & Interfaces*, 2014, **6**, 5050-5055.
8. X. J. Ma, L. B. Kong, W. B. Zhang, M. C. Liu, Y. C. Luo and L. Kang, *RSC Advances*, 2014, **4**, 17884-17890.
9. W. Hong, J. Q. Wang, P. W. Gong, J. F. Sun, L. Y. Niu, Z. G. Yang, Z. F. Wang and S. R. Yang, *Journal of Power Sources*, 2014, **270**, 516-525.
10. L. Q. Mai, F. Yang, Y. L. Zhao, X. Xu, L. Xu and Y. Z. Luo, *Nature Communications*, 2011, **2**, 381.
11. D. Guo, W. J. Ren, Z. Chen, M. L. Mao, Q. H. Li and T. H. Wang, *RSC Advances*, 2015, **5**, 10681-10687.
12. D. P. Cai, B. Liu, D. D. Wang, L. L. Wang, Y. Liu, H. Li, Y. R. Wang, Q. H. Li and T. H. Wang, *Journal of Materials Chemistry A*, 2014, **2**, 4954-4960.